Progress in Physics of Applied Materials

Magnetic properties of Co$_{0.9}$Cd$_{0.1}$Fe$_{1.9}$X$_{0.1}$O$_4$ (X = Cr, Yb) nanoparticles prepared by hydrothermal method

H. Ghorbani, M. Eshraghi*, A. Sabouridodaran*

Department of Physics, Payam Noor University, Iran

A R T I C L E   I N F O

A B S T R A C T

The present study investigated the cadmium-cobalt ferrite nanoparticles doped with chromium and ytterbium ions synthesized using the hydrothermal method. We analysed the samples by X-ray diffraction (XRD), Field Emission Scanning Electron Microscope (FESEM), and vibrating Sample Magnetometer devices (VSM). XRD confirmed the formation of an almost pure spinel structure. FESEM-obtained micrographs showed spherical shapes for nanoparticles and by using ImageJ software, an average particle size of about 40 nm was obtained. The saturation magnetization, the remnant magnetization, and the coercivity field were estimated using the hysteresis loop of the samples. The maximum coercivity field (815 Oe)was obtained in the sample doped with ytterbium. This could be due to enhancing the spin-orbit coupling and magnetocrystalline anisotropy constant of the cadmium-cobalt ferrite sample with ytterbium doping. The saturation magnetization decreased with the doping of both ions due to the lower magnetic moment of the doped ions compared to the Fe ion.

1. Introduction

Spinel ferrites, with the general formula MFe$_2$O$_4$ (where M is a divalent metal ion), are attractive types of magnetic materials with different applications in industry and science. One of the reasons that magnetic ferrites have achieved such wide applications is the possibility of diversifying their composition and optimizing their properties by different preparation methods. Some of these methods include; changes in their construction method, changes in effective parameters in preparation (including temperature, time, pressure, etc.), doping ferrites with different ions, etc. The Cobalt ferrite (CoFe$_2$O$_4$) that is one of the spinel ferrites, is considered as a hard magnetic material due to its high coercivity field and consequently having a wide hysteresis loop, and attracted the attention of researchers due to its attractive properties and has allocated a lot of research to itself [1-3]. Magnetic anisotropy field and consequently huge coercivity field, chemical stability, and high mechanical stiffness, relatively large saturation magnetization, etc. are among the properties that have caused to use of this substance in medical sciences (use in imaging, distribution, and targeted delivery of drugs, hyperthermia, etc.), military sciences (radars, etc.), computer sciences (magnetic memories, etc.) and various other sciences and industries[4-8]. It has been said that one of the methods to optimize the properties of ferrites is doping with different ions because a small amount of an external ion in the composition of ferrites can

significantly change their properties [9-11]. Among these, non-magnetic metal ions such as zinc and cadmium are of particular importance because they do not exhibit magnetic moment and can disturb the magnetic moment's equilibrium in the ferrite composition [9-19]. In these ions whose electron configuration is [Ar]3d^{10}4S^2 for Zn, and [Kr]4d^{10}5S^2 for Cd, when the electrons of the valence layer (S orbital) are removed, their electron configuration becomes [Ar]3d^{10} for Zn^{+2}, and [Kr]4d^{10} for Cd^{+2}. In this case, it is observed that all the orbitals of the current valence layer, which are the d orbitals, are full, and the electrons are paired. This is why these ions do not have a pure magnetic moment and are called non-magnetic ions.

In a study by Kaur et al. cobalt ferrite nanoparticles were doped with Zn^{+2} and Cd^{+2} ions, and their structural, thermal, and magnetic properties were investigated [20]. By studying the results of that research, it was observed that the magnetization of the doped samples increased compared to the sample without doping, but the magnetization increasing in the Cd^{+2} doped sample was greater than that of the sample doped with Zn^{+2}. Therefore, in this research cadmium cobalt ferrite was considered for further investigation.

Another attractive class of ions that scientists has used more in their recent research for doping in ferrite compounds is the rare-earth ions. In these ions, due to the inner 4f electron layer, there is an unquenched angular momentum that results in a significant spin- orbit interaction, thus having a high magnetocrystalline

* Corresponding author(s). Tel.: +98-913-2170496
E-mail address: eshraghi@nj.isfpnu.ac.ir, sabouri@pnu.ac.ir

anisotropy. Therefore, it is expected that if these ions are added to the ferrites, they can increase the coercivity field (HC) [21]. In a study by Routray et al., after doping of La in cobalt ferrite, the HC increased from 1950Oe for sample x=0 to 3300 Oe for sample x=0.1 [22]. Also, Almessiereet al. reported that by doping 4% Tm ion in cobalt ferrite, it increased nearly 60% [23]. In the study of Bulai et al., the substitution of 8 ions from the rare earth group was compared with the pure sample. For all the doped samples, HC was higher than the undoped sample [24]. Based on the above data, we selected the Yb^{+3} from the rare earth group for our research, which in recent research is less used than the other ions of this group, for doping in ferrites. On the other hand, by studying recent articles, it was observed that in some cases, Cr^{+3} doping in the ferrite compounds, including cobalt ferrite, leads to an increase of coercivity field. In a study by Zhang et al., for chromium-doped cobalt ferrite ($CoCr_xFe_{2-x}O_4$) samples, the maximum coercivity field value was 6400 Oe in sample x=0.6. [25].

With that in mind, another ion we chose for doping in our sample is Cr. Thus, in this study, we synthesized samples of cobalt-cadmium ferrite doped with Cr^{+3} and Yb^{+3} (separately) with a doping value of 0.1 {$Co_{0.9}Cd_{0.1}Fe_{1.9}x_{0.1}O_4$(x=Cr, Yb)} by hydrothermal method to see if doping both Yb and Cr ions can affect simultaneously on the coercivity field to increase. After confirming the formation of the spinel structures, we investigated their magnetic properties. Our results show that Yb doping significantly increases HC.

2. Experimental

In this research, the $Co_{0.9}Cd_{0.1}Fe_2O_4$, $Co_{0.9}Cd_{0.1}Fe_{1.9}Cr_{0.1}O_4$, and $Co_{0.9}Cd_{0.1}Fe_{1.9}Yb_{0.1}O_4$ nanoparticles were synthesized via the hydrothermal method. The following materials were used as starting materials to make the samples: iron(III) chloride hexahydrate ($FeCl_3$-$6H_2O$), cobalt chloride hexahydrate ($CoCl_2$-$6H_2O$), cadmium chloride ($CdCl_2$-$2.5H_2O$), ytterbium chloride hexahydrate ($YbCl_3$-$6H_2O$), and sodium hydroxide (NaOH). After weighing the stoichiometric amounts of the metal salts, they were dissolved in deionized water. Simultaneously, a 0.5 molar sodium hydroxide solution was prepared and gently added to the metals salt solution. They were then stirred for 30 minutes on a magnetic stirrer to obtain a homogeneous solution. Once the dark and homogeneous precursor was obtained, the precursor was poured into an autoclave and heated at 250°C for two hours. After cooling, the material was washed with deionized water and ethanol. To obtain the final samples, the washed material was dried on a heater at 70° C for 3 hours.

After preparing the samples X-ray diffractometer was employed using a Cu-Kα (λ=1.5406 A°) radiation in the range of 2θ=20-80° as a source to confirm the formation of the spinel structure. The surface morphology of the annealed powders was determined by field emission scanning electron microscopy (FE-SEM). Then, to study the magnetic properties of the samples, vibrational sample magnetometry analysis (VSM, Meghnatis Daghigh Kavir Co., Iran) was used.

Explanation: The samples were named as:

(Cd)→$Co_{0.9}Cd_{0.1}Fe_2O_4$ and(Cd-Cr)→$Co_{0.9}Cd_{0.1}Fe_{1.9}Cr_{0.1}O_4$ and (Cd-Yb)→$Co_{0.9}Cd_{0.1}Fe_{1.9}Yb_{0.1}O_4$.

3. Results and Discussion

The XRD patterns of samples are shown in Fig. 1. Comparing these patterns with the standard cobalt ferrite card (No. 22-1086)[26,27], we see no impurity peaks in the XRD pattern of samples. Reflections were observed from (220), (331), (400), (422), (511), and (440), planes indicating the formation of a single-phase cubic spinel structure for synthesized samples.
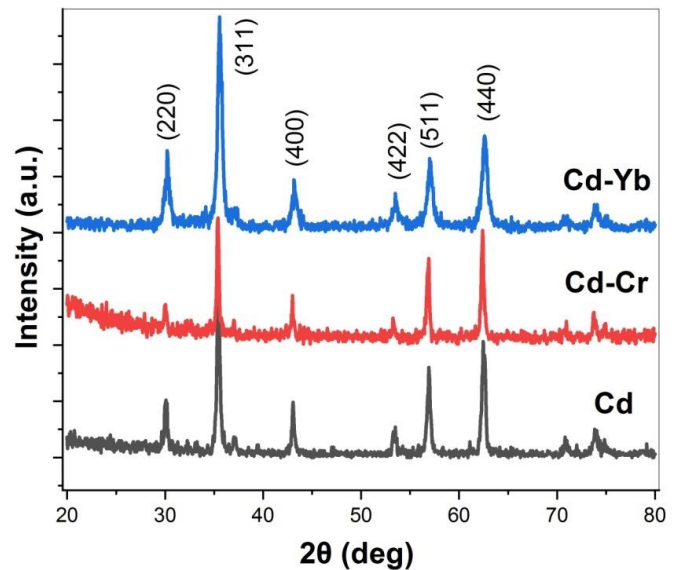

Fig. 1. X-ray diffraction pattern of samples.

We further performed the Rietveld refinement of the XRD data using Fullprof-Suite software, which confirmed the material belongs to the $Fd3m$ space group. Using $a = d_{hkl}\sqrt{h^2 + k^2 + l^2}$ ($d_{hkl}$is the lattice spacing, and hkl are Miller indexes) and after Rietveld refinement, we obtained the lattice parameter for the samples, as shown in Table 1. Let's look at the ionic radius of the ions. The lattice parameter did not change because the ionic radius of Cr^{+3} (62 pm) and Fe^{+3} (60 pm) are close. But by considering the sizeable ionic radius difference between Fe^{+3} andYb^{+3}(87 pm), the lattice parameter decreased significantly by Yb doping. The X-ray density of prepared samples calculated from $\rho_{XRD} = \frac{8M}{N_A a^3}$ and they are listed in table 1. In this equation, N_A is Avogadro's number, M is the formula mass of the sample, and the number 8 is due to the number of units of each sample (Cd, Cd-Cd, Cd-Yb) per unit cell. [28]. The significant increase of X-ray density in the Yb doped sample is due to the big difference between the atomic weight of Yb (173.05 amu) and Fe (55.84 amu) ions.

To obtain images and observe the morphology of the samples, we subjected them to field emission scanning electron microscopy (FE-SEM) analysis. These images are shown in Fig. 2. The images obtained by FE-SEM analysis show that the cadmium-cobalt ferrite nanoparticles are almost spherical and uniformly distributed.

By using ImageJ software, the average particle size of samples was estimated to be about 40nm. Table 1 lists the average particle sizes obtained from the FE-SEM images.
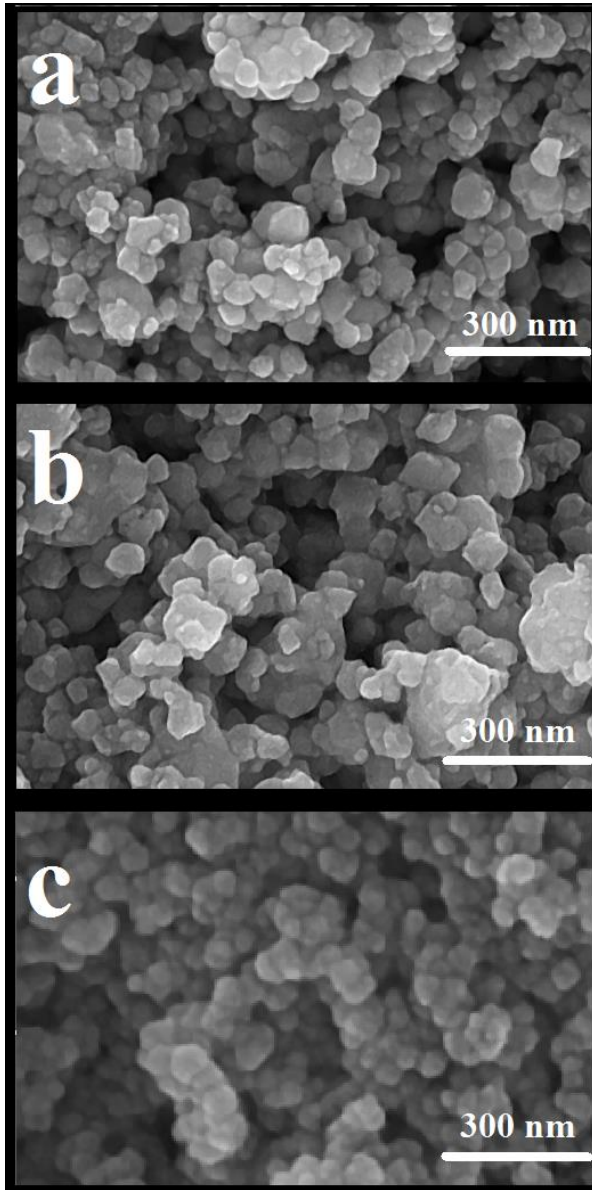

Fig. 2. FE-SEM images of samples a)Cd, b)Cd-Cr,c)Cd-Yb..

Table 1
lattice parameter, particle size (from FE-SEM images), and X-ray density of the samples.

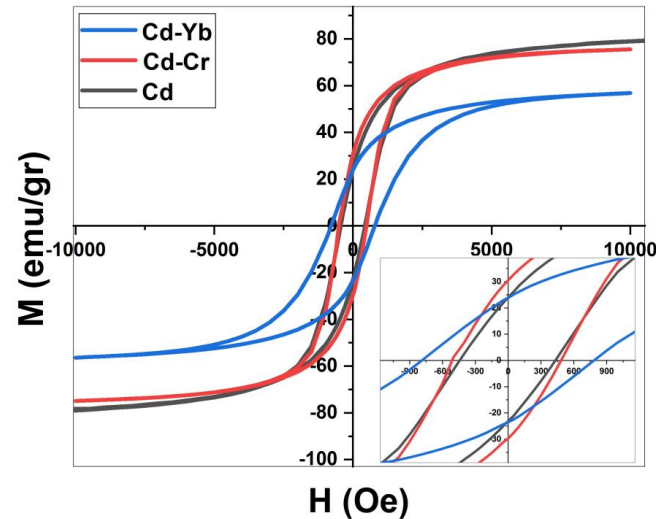| sample	Cd	Cd-Cr	Cd-Yb
a (Å)	8.41	8.41	8.35
D_FESEM (nm)	40	41	40
ρ_XRD (g/cm3)	5.81	5.80	6.31

Fig. 3. hysteresis loop of the samples at room temperature.
Inset shows the magnetization curve with a field range of -1 to +1 kOe

The hysteresis loop of the samples is shown in Fig. 3. The magnetic parameters obtained with the help of this diagram are listed in Table 2.

As we know, cobalt ferrite has an inverse spinel structure. In other words, divalent ions are located in octahedral (B) sites. Thus half of the trivalent ions are in octahedral (B) sites, and the other half are in tetrahedral (A) sites. For this reason, the magnetic property of cobalt ferrite is mainly due to the divalent ions of cobalt, which are in the octahedral sites. Because the magnetic moments of the trivalent iron ions, which are unparallel in the octahedral and tetrahedral sites, neutralize each other's magnetic properties (see Fig. 4a). When one of the non-magnetic ions (eg Cd^{+2}) enters the cobalt ferrite composition, although it replaces Co^{+2} in the octahedral sites, it prefers to sit in the tetrahedral sites. Thus, as much as Cd^{+2} entrees the compound, the same Fe^{+3} transfers from the octahedral to the tetrahedral position (see Fig. 4b). As we know, according to NeilNeel's theory, the theoretical magnetic moment is given by the equation:

$$n_B^{Cal} = M_B - M_A \tag{1}$$

where M_A and M_B are the A-site and B-site sub-lattice magnetic moments estimated from the magnetic moment of each ion in μ_B (Bohr magneton) (5, 3, 0 for Fe^{+3}, Co^{+2}, and Cd^{+2}, respectively) [10,28-29]. With cadmium doping, the magnetic moment of the A-sites reduces by $5\mu_B$, equivalent to the magnetic moment of Fe^{+3} that is removed from the tetrahedral position. Instead, the magnetic moment of the B-sites increases by $2\mu_B$. Due to the replacement of Fe^{+3} instead of Co^{+2} in these sites, whose magnetic moment difference is equal to $5\mu_B$-$3\mu_B$ = $2\mu_B$. Therefore, the total magnetic moment, the difference between the A and B-sites' magnetic moment, increases the compound's magnetization.
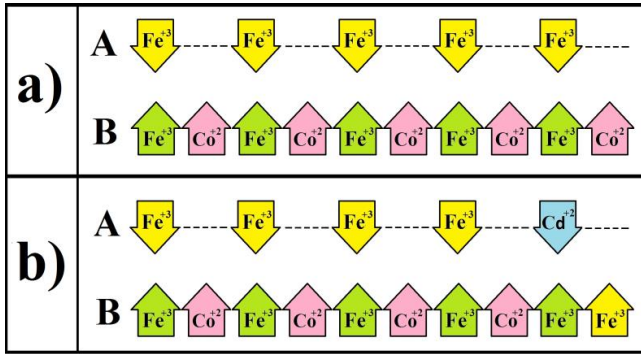
Fig. 4. a) Inverse spinel structure of cobalt ferrite b) Mixed spinel structure of cobalt ferrite doped with cadmium.

The structure of cadmium-cobalt ferrite and how ions are located in tetrahedral and octahedral sites can be represented in Fig. 4b. Now consider adding Cr^{+3} or Yb^{+3} to this structure. We know that Cr^{+3} replaces Fe^{+3} when it enters the composition, preferring to sit in octahedral sites. The magnetic moment of Cr^{+3} is $3\mu_B$, and the magnetic moment of Fe^{+3} is $5\mu_B$. By locating the Cr^{+3} in the octahedral sites, the value of $3\mu_B$ is added to the magnetic moment of the octahedral sites. Because Fe^{+3} is removed from the octahedral sites, the magnetic moment of B-sites reduces by $5\mu_B$, so the net magnetic moment of B-sites decreases by $2\mu_B$, and thus the total magnetic moment decreases. As a result, as shown in table 2, in the Cr^{+3} doped sample, saturation magnetization (Ms) decreased compared to the undoped sample.

Similarly, due to the lower magnetic moment of $Yb^{+3}(4\mu_B)$ compared to $Fe^{+3}(5\mu_B)$, the saturation magnetization of the sample doped with Yb decreased, as shown in Fig. 3 and Table 2. According to equation 1, as previously described, we obtained the theoretical magnetic moment of the samples, and the results are shown in Table 2. The experimental magnetic moment of the samples is also obtained with the help of the below equation [30, 31]:

$$n_B^{exp} = \frac{M_S(emu/g) \times M_W(gmol^{-1})}{\mu_B(^J/_T) \times N_A(mol^{-1}) \times 10^3} = \frac{M_W(g) \times M_S(emu/g)}{5585} \qquad (2)$$

Where M_W is the molecular weight of the samples and M_S is the amount of saturation magnetization. In fact, with the help of the values of Bohr magneton (μ_B = 9.274×10^{-24} J/T) and Avogadro number (N_A=6.0221409×10^{23} mol^{-1}) values and using the conversion factor of 1 emu=10^{-3} J/T, the corresponding simplification is done. The calculation result is presented in Table 2. As can be seen from the data in Table 2, the calculated value,n_B^{cal} is different from the value of n_B^{exp} . One reason for this could be the difference in particle size of the samples. Another reason that can be mentioned is the distribution of cations in octahedral and tetrahedral sites. There is also another factor that should be considered. As mentioned, by substituting Cd^{+2} ions in the cobalt ferrite composition, the symmetry of the Fe^{+3} ions at the octahedral and tetrahedral sites is disturbed, and we saw that the Fe^{+3} ions no longer neutralize each other's effects. We then substituted Cr^{+3} or Yb^{+3} ions for Fe^{+3} ions in the resulting composition (i.e., cadmium-cobalt ferrite). Due to the addition of these new ions and the fact that each of these ions has a different magnetic moment

from its neighbor, the magnetic moment of ions located in the octahedral and tetrahedral sites can no longer be considered antiparallel. Evidence of this is the difference in the value of the experimental magnetic moment and the theoretical magnetic moment[32]. For this reason, Neel's two-sublattice model is no longer able to estimate the magnetic moment of the samples, and another model, called the Yaffet-Kittel's (Y-K) three-sublattice model, must be used to calculate the magnetic moment of the samples. In this model, the magnetic moment is calculated by equation (3)[32, 33]:

$$n_B = M_B cos\alpha - M_A \qquad (3)$$

According to this model, the magnetic moment of the B-sites is composed of two components B1 and B2, that have equal value with the Y-K angle (α_{y-k}) between them. This is due to the difference in the value of the theoretical magnetic moment and experimental magnetic moment. [33-37] (see Fig. 5). We calculated the angle α_{y-k} by equation (3). The results are shown in Table 2. As can be seen, the Y-K angle increased in the doped samples confirming the reduced magnetization in these samples compared to the cadmium-cobalt ferrite sample. Because the higher α_{y-k} results in higher spin canting on B-site, the total M decreases[33,36-37]. By Yb and Cr doping, the number of Fe ions decreases on B-site. Thus, the strength of the exchange interaction between the ions may decrease on the B-site, which result in the spin canting of the ions on A-site and then decrease the net magnetic moments. The higher Yafet-Kittle angle observed in Yb substitution than Cr substitution could be due to the weaker exchange interaction between Yb and Fe ions in the B-sites(Yb 4f electrons are relatively localized) compared to the Cr –Fe ions interaction.
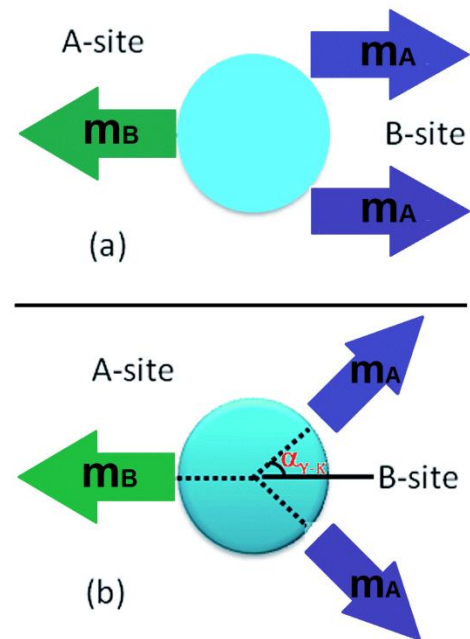

Fig.5. The orientation of magnetic moment at A and B-sites. (a) Neel'smodel (Linear) (b) Yaffet-Kittel's Model (Nonlinear).

Table 2
Magnetic parameters of the samples

sample	Cd	Cd-Cr	Cd-Yb
Ms (emu/g)	81	76	59
Hc (Oe)	430	490	815
Mr (emu/g)	24	31	25
n_B^{exp} (μB)	3.48	3.26	2.73
n_B^{cal} (μB)	3.7	3.5	2.6
R (Mr/Ms)	0.3	0.41	0.44
K (erg/g) ×105	2.02	2.06	12.29
$\alpha y\text{-}k$ (deg)	13.3	14.1	26.8

According to the data in Table 2, we can see an almost double increase in the coercivity field of samples doped with Yb^{+3} compared to the undoped sample. To justify this, we consider the electron configuration of rare-earth ions. In this group of ions, the 4f orbital layer, closer to the core than the 5d orbital, is not filling. Therefore, in these ions, the rate of spin-orbit interaction is high due to the unquenched orbital angular momentum. Since the magnetocrystalline anisotropy mainly originates from the spin-orbit interaction thus its value is significant in this group of ions[24,38]. It is well known that as the magnetic anisotropy increases, the coercivity field increases. This is why the coercivity field increases with Yb^{+3} doping. Such behavior has been reported in several studies [24,39]. The increase of the H_C in the Cd-Cr sample could be due to the difference in the anisotropy coefficient of the Cr with Fe. As described, the coercivity field (H_C) is directly related to the anisotropy coefficient, and the higher the anisotropy coefficient, the higher the coercivity field. We further

calculated the remanence ratio that is equal to the ratio of the remanent magnetization to the saturation magnetization ($R = Mr/Ms$) [40, 41]. The calculated values of R are given in Table 2. According to Stoner-Wolfarth's (S-W) theory, if R is about 0.83, it is related to cubic anisotropy, and if about 0.5, related to uniaxial anisotropy. It can be seen from Table 2 that the R values of the samples are in the range of $R\leq 0.5$, indicating a single magnetic domain with uniaxial anisotropy. To obtain the samples' anisotropy constant (K), we can use the relationship between the magnetization and the applied field. This relationship is shown by Equation (4) [42]:

$$M = M_S \left(1 - \frac{\alpha}{H} - \frac{\beta}{H^2}\right) + \chi H \tag{4}$$

In this equation α, β and χ are constant, and M_S is the saturation magnetization. The first constant (α), which is related to micro-stresses (or local stress due to crystal defects), shows itself only in a specific and small area of the field and can be ignored in high fields [42]. Also, the χ-constant, which is related to the increased field in the spontaneous magnetic domain and is known as the paramagnetism-like term, is ignored at temperatures below the Curie temperature[43,44]. So the equation (4) can be roughly replaced by [45-47]:

$$M = M_s \left(1 - \frac{\beta}{H^2}\right) \tag{5}$$

The term that contains β is related to effective magnetic anisotropy, K, and can be written as[47-50]:

$$K = M_S \sqrt{\frac{15\beta}{4}} \tag{6}$$

To use equation (6), we must first obtain the β constant by plotting the M diagram versus $1/H^2$, and then obtain the anisotropy constant(K) of the samples using equation (6). The magnetization diagram (M) in terms of $1/H^2$ for all samples is shown in Fig. 6. The values obtained for K are listed in Table 2. According to the obtained values, anisotropy constants increased by Yb doping due to the stronger spin-orbit coupling of Yb compared to Fe.
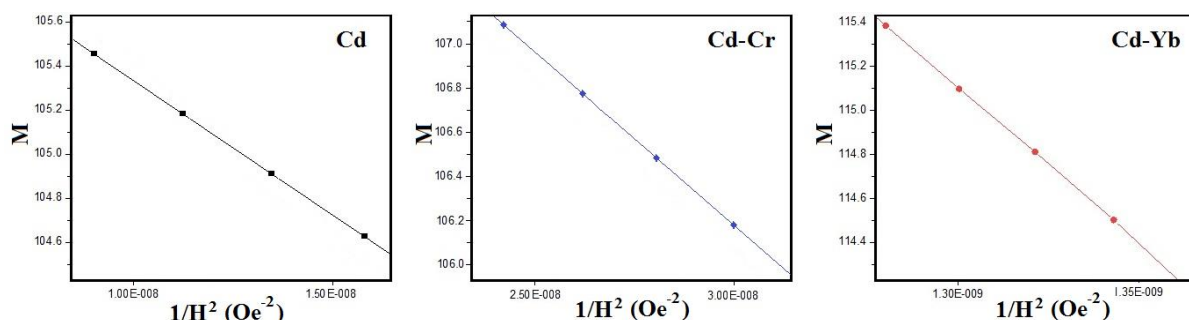

Fig. 6. The M diagram versus the $1/H^2$ for all samples

4. Conclusion

In this study, samples of cadmium-cobalt ferrite nanoparticles were synthesized with chromium and ytterbium doping by using the hydrothermal method. XRD analysis of the samples confirmed the formation of spinel structure. VSM analysis showed that saturation magnetization reduced by Cr and Yb doping in cadmium-cobalt ferrite nanoparticle samples. The coercivity field of the doped samples increased due to the increase of the spin-orbit coupling and the magnetocrystalline anisotropy constant.

Acknowledgements

References

[1] P.P. Goswam, H.A. Choudhury, S. Chakma, V.S. Moholkar, Sonochemical Synthesis of Cobalt Ferrite Nanoparticles, International Journal of Chemical Engineering, 2013 (2013) 934234.

[2] N. Somaiah, T.V. Jayaraman, P.A. Joy, D. Das, Magnetic and magnetoelastic properties of Zn doped cobalt-ferrites $CoFe_{2-x}Zn_xO_4$(x = 0, 0.1,0.2, and 0.3), J. Magnetism and Magnetic Materials, 324-14 (2012), 2286-2291.

[3] S. Singhal, T. Namgyal, S. Bansal, K. Chandra, Effect of Zn Substitution on the Magnetic Properties of Cobalt Ferrite Nano Particles Prepared Via Sol-Gel Route, J. Electromagnetic Analysis and Applications, (2010), 2, 376-381.

[4] R. Bhowmik, R. Ranganathan, B. Ghosh , S. Kumar, S. Chattopadhyay, Magnetic ordering and electrical resistivity in $Co_{0.2}Zn_{0.8}Fe_2O_4$ spinel oxide, J. Alloys and Compounds, 456 (2008) 348-352.

[5] A. Daigle, J. Modest, A. L. Geiler, S. Gillette, Y. Chen, M. Geiler, B. Hu, S. Kim, K. Stopher, V. G. Harris, Structure, morphology and magnetic properties of $Mg_{(x)}Zn_{(1-x)}Fe_2O_4$ ferrites prepared by polyol and aqueous co-precipitation methods: a low-toxicity alternative to $Ni_{(x)}Zn_{(1-x)}Fe_2O_4$ ferrites, J. Nanotechnology, (2011), 22(30), 305708.

[6] C. Upadhyay, D. Mishra, H. Verma, S. Anand, R. Das, Effect of preparation conditions on formation of nanophase Ni–Zn ferrites through hydrothermal technique, J. Magn. Magn. Mater, 260 (2003) 188-194.

[7] P. Coppola, F.G. da Silva, G. Gomide, F.L.O. Paula, A.F.C. Campos, R. Perzynski, C. Kern, J. Depeyrot, R. Aquino, Hydrothermal synthesis of mixed zinc–cobalt ferrite nanoparticles: structural and magnetic properties, J. Nanoparticle Research, 18 (2016) 138.

[8] F. Saffari, P. Kameli, M. Rahimi, H. Ahmadvand, H. Salamati, Effects of Co-substitution on the structural and magnetic properties of $NiCo_xFe_{2-x}O_4$ ferrite nanoparticles, J. Ceramics International, 41 (2015) 7352-7358.

[9] M. Shelar, P. Jadhav, S. Chougule, M. Mallapur, B. Chougule, Structural and electrical properties of nickel cadmium ferrites prepared through self-propagating auto combustion method, J. Alloys and Compounds, 476 (2009) 760-764.

[10] M. Rahimi, M. Eshraghi, P. Kameli, Structural and magnetic characterizations of Cd substituted nickel ferrite nanoparticles. *Ceramics international*, *40* (2014) 15569-15575.

[11] S.P. Dalawai, T.J. Shinde, A.B. Gadkarai, P.N. Vasambekar, Structural properties of Cd–Co ferrites, J. Indian Academy of Sciences, 36 (2013) 919-922 .

[12] G. Tang, D. Ji, Y. Yao, S. Liu, Z. Li ,W. Qi, et al., Quantum-mechanical method for estimating ion distributions in spinel ferrites, J. Appl. Phys. Lett, 98(2011), 072511.

[13] M. Kaur, S. Rana, P.S. Tarsikka, Comparative analysis of cadmium doped magnesium ferrite $Mg_{1-x}Cd_xFe_2O_4$ (x= 0.0, 0.2, 0.4, 0.6) nanoparticles, J. Ceram. Int. 38 (2012) 4319-4323.

[14] S.P. Jadhav, B.G. Toksha, K.M. Jadhav, N.D. Shinde, Effect of cadmium substitution on structural and magnetic properties of nanosized nickel ferrite, Chin. J. Chem. Phys. 23 (2010) 459.

[15] M. Karanjkar, N. Tarwal, A. Vaigankar, P. Patil, Structural, Mössbauer and electrical properties of nickel cadmium ferrites, J. Ceram. Inter. 39 (2013) 1757-1764.

[16] Y.H. Hou, Y.J. Zhao, Z.W. Liu, H.Y. Yu, X.C. Zhong, W.Q. Qiu, D.C. Zeng, L.S. Wen, First-principles investigations of Zn (Cd) doping effects on the electronic structure and magnetic properties of CoFe2O4, *Journal of Applied Physics*, *109* (2011) 07A502.

[17] S.S. Jadhav, S.E. Shirsath, S.M. Patange, K. Jadhav, Effect of Zn substitution on magnetic properties of nanocrystalline cobalt ferrite, J. Appl. Phys. 108 (2010) 093920-093926.

[18] A. Gadkari, T. Shinde, P. Vasambekar, Structural and magnetic properties of nanocrystalline Mg–Cd ferrites prepared by oxalate coprecipitation method, J. Mater. Sci.:Mater. Electron. 21 (2010) 96-103.

[19] A.M. Abdeen, O.M. Hemeda, E.E. Assem, M.M. El-Sehly, Structural, electrical and transport phenomena of Co ferrite substituted by Cd, J. Magnetism and Magnetic Materials 238 (2002) 75-83.

[20] H. Ghorbani, M. Eshraghi, Investigation of chromium doping effect on the structural and magnetic properties of $MnFe_{2-x}Cr_xO_4$ ferrite nanoparticles, J. Research on Many-body Systems, 6 (2016) 1-9.

[21] G. Goya, T. Berquo, F. Fonseca, M. Morales, Static and dynamic magnetic properties of spherical magnetite nanoparticles, J. Appl. Phys. 94 (2003) 3520.

[22] H. Kaur, A. Singh, V. Kumar, D.S. Ahlawat, Structural, thermal and magnetic investigations of cobalt ferrite doped with Zn^{2+} and Cd^{2+} synthesized by auto combustion method, J. Magnetism and Magnetic Materials 474 (2019) 505–511 .

[23] K.P. Remya, S. Amirthapandian, M.M. Raja, C. Viswanathan, N. Ponpandian, Effect of Yb substitution on room temperature magnetic and dielectric properties of bismuth ferrite nanoparticles, J. Appl. Phys. 120 (2016), 134304.

[24] K.L. Routray, S. Saha, D. Behera, Rare-earth (La^{+3}) substitution induced changes in the structural, dielectric and magnetic properties of nano-$CoFe_2O_4$For high-frequency and magneto-recording devices, J. Applied Physics A, (2019) 125:328.

     H. Ghorbani/ Progress in Physics of Applied Materials 1 (2021) 50-56

[25] M. A. Almessiere, Y. Slimani, A. D. Korkmaz, S. Guner, M. Sertkol, S. E. Shirsath, A. Baykal, Structural, optical and magnetic properties of Tm^{3+} substituted cobalt spinel ferrites synthesized via sonochemical approach, J. Ultrasonics sonochemistry, (2019), 54, 1-10.

[26] G. Bulai, L. Diamandescu, I. Dumitru, S. Gurlui, M. Feder, O.F. Caltun, Effect of rare earth substitution in cobalt ferrite bulk materials, J. Magn. Magn. Materials 390(2015), 123–131.

[27] W. Zhang, X. Zuo, D. Zhang, C. Wu, S. R. P. Silva, Cr^{3+} substituted spinel ferrite nanoparticles with high coercivity, J. Nanotechnology, 27 (2016) 245707.

[28] H. Khedri, A. Gholizadeh, Experimental comparison of structural, magnetic and elastic properties of $M_{0.3}Cu_{0.2}Zn_{0.5}Fe_2O_4$ (M = Cu, Mn, Fe, Co, Ni, Mg) nanoparticles, J.Applied Physics A (2019) 125:709.

[29] S.J. Olusegun, E.T.F. Freitas, L.R.S. Lara, H.O. Stumpf, N.D.S. Mohallem, Effect of drying process and calcination on the structural and magnetic properties of cobalt ferrite, J. Ceramics International 45 (2019) 8734–8743.

[30] A. Manohar, D.D. Geleta, C. Krishnamoorthi, J. Lee, Synthesis, characterization and magnetic hyperthermia properties of nearly monodisperse $CoFe_2O_4$ nanoparticles, J. Ceramics International , 46 (2020) 28035-28041.

[31] N. Shamgani, A. Gholizadeh, Structural, magnetic and elastic properties of $Mn_{0.3-x}Mg_xCu_{0.2}Zn_{0.5}Fe_3O_4$ nanoparticles, J.Ceramics International 45 (2019) 239–246.

[32] A. Gholizadeh, A comparative study of physical properties in Fe_3O_4 nanoparticles prepared by coprecipitation and citrate methods. *Journal of the american ceramic society*, *100* (2017) 3577-3588.

[33] S. Karimi , P. Kameli , H. Ahmadvand , H. Salamati, Effects of Zn-Cr-substitution on the structural and magnetic properties of $Ni_{1-x}Zn_xFe_{2-x}Cr_xO_4$ ferrites, J. Ceramics International 42 (2016) 16948–16955.

[34] R. Topkaya , A. Baykal , A. Demir , Yafet–Kittel-type magnetic order in Zn-substituted cobaltferrite nanoparticles with uniaxial anisotropy, J.Nanopart Res (2013) 15:1359.

[35] G. Alvarez, H. Montiel, J.F. Barron, M.P. Gutierrez , R. Zamorano, Yafet–Kittel-type magnetic orderingin $Ni_{0.35}Zn_{0.65}Fe_2O_4$ ferrite detected by magnetosensitive microwave absorption measurements, J. Magnetism and Magnetic Materials , 322 (2010) 348–352 .

[36] Y. Yafet, C. Kittel, Antiferromagnetic arrangements in ferrites, J. Phys. Rev. 87 (1952) 290.

[37] C. Choodamani, G.P. Nagabhushana, S. Ashoka, B. Daruka-Prasad, B. Rudraswamy, G.T. Chandrappa, Structural and magnetic studies of $Mg_{1-x}Zn_xFe_2O_4$ nanoparticles prepared by a solution combustion method, J. Alloys and Compounds, 578(2013) 103-109.

[38] M. Beyranvand, A. Gholizadeh, Structural, magnetic, elastic, and dielectric properties of $Mn_{0.3-x}Cd_xCu_{0.2}Zn_{0.5}Fe_2O_4$ nanoparticles. *Journal of Materials Science: Materials in Electronics*, *31* (2020) 5124-5140.

[39] M. Yousaf, M.N. Akhtar, B. Wang, A. Noor, Preparations, optical, structural, conductive and magnetic evaluations of RE's (Pr, Y, Gd, Ho, Yb) doped spinel nanoferrites, J. Ceramics International 46-4 (2020), 4280-4288.

[40] S.M. Peymani-Motlagh, A. Sobhani-Nasab, M. Rostami, H. Sobati, M. Eghbali-Arani, M. Fasihi-Ramandi, M. R. Ganjali, M. Rahimi-Nasrabad, Assessing the magnetic, cytotoxic and photocatalytic influence of incorporating Yb^{3+} or Pr^{3+} ions in cobalt–nickel ferrite, J. Materials Science: Materials in Electronics 30(2019), 6902–6909.

[41] M. Yehia, A. Hashhash, Structural and magnetic study of Sm doped $NiFe_2O_4$Nanoparticles, J. Materials Science: Materials in Electronics, (2019), 10854-019-00988-9.

[42] V. Turchenko, V.G. Kostishin, S. Trukhanov, F. Damay , M.B.B. Bozzo, I. Fina, V.V. Burkhovetsky, S. Polosan, M.V. Zdorovets, A.L. Kozlovskiy, K.A. Astapovich, A. Trukhanov, Structural features, magnetic and ferroelectric properties of $SrFe_{10.8}In_{1.2}O_{19}$ compound, J. Materials Research Bulletin 138(2021) 111236.

[43] D.E. Grady, Origin of the Linear Term in the Expression for the Approach to Saturation in Ferromagnetic Materials, J. Phys. Rev. B, 4 (1971) 3982.

[44] A. Arrott, Dzialoshinski-Moriya Interactions About Defects in Antiferromagnetic and Ferromagnetic Materials, J. Applied Physics, 34 (1963) 1108.

[45] A. Aharoni, One-Dimensional Theory of the Parasitic Paramagnetism Term in the Approach to Saturation, J. Phys. Rev. 132 (1963)105.

[46] N. Modaresi, R. Afzalzadeh, B. Aslibeiki, P. Kameli, Competition between the Impact of Cation Distribution and Crystallite Size on Properties of $Mn_xFe_{3-x}O_4$ Nanoparticles Synthesized at Room Temperature, J. ceramics Int, *43*(2017) 15381-15391.

[47] H. Ghorbani, M. Eshraghi, A. S. Dodaran, P. Kameli, S. Protasowicki, C. Johnson, D. Vashaee, Effect of Yb doping on the structural and magnetic properties of cobalt ferrite nanoparticles, J. Materials Research Bulletin, 147(2022) 111642.

[48] B. Yalcin, S. Ozcelik, K. Icin, K.Senturk, B. Ozcelik, L. Arda, Structural, optical, magnetic, photocatalytic activity and related biological effects of $CoFe_2O_4$ ferrite nanoparticles, J. Mater Sci: Mater Electron 32 (2021) 13068–13080.

[49] H. Zhang, D. Zeng, Z. Liu, The law of approach to saturation in ferromagnets originating from the magnetocrystalline anisotropy, J. Magn. Magn. Materials 322 (2010) 2375–2380.

[50] B.D. Cullity, C.D. Graham, Introduction to Magnetic Materials, John Wiley & Sons, (2011).